New insights into the magnetic properties of $LaErO_3$, $(La_{0.5}Er_{0.5})_2O_3$ and $(La_{0.5}Dy_{0.5})_2O_3$ oxides

2016 J. Phys.: Condens. Matter 28 066003

(http://iopscience.iop.org/0953-8984/28/6/066003)

IOP Publishing Journal of Physics: Condensed Matter
J. Phys.: Condens. Matter **28** (2016) 066003 (9pp) doi:10.1088/0953-8984/28/6/066003

New insights into the magnetic properties of $LaErO_3$, $(La_{0.5}Er_{0.5})_2O_3$ and $(La_{0.5}Dy_{0.5})_2O_3$ oxides

A Martinelli[1], C Artini[2,3] and L Keller[4]

[1] SPIN-CNR, Corso Perrone 24, 16152 Genova, Italy
[2] Department of Chemistry and Industrial Chemistry, University of Genova, Via Dodecaneso 31, 16146 Genova, Italy
[3] CNR-IENI, Via De Marini 6, 16149 Genova, Italy
[4] Laboratory for Neutron Scattering and Imaging, Paul Scherrer Institut, 5232 Villigen PSI, Switzerland

E-mail: alberto.martinelli@spin.cnr.it

Received 6 October 2015, revised 24 December 2015
Accepted for publication 4 January 2016
Published 21 January 2016

Abstract

Orthorhombic $LaErO_3$ and cubic $(La_{0.5}Ln_{0.5})_2O_3$ oxides (*Ln*: Er, Dy) were examined by neutron powder diffraction between 1.5 K and 15 K in order to investigate their crystallographic and magnetic structures. At 1.5 K both $LaErO_3$ and $(La_{0.5}Er_{0.5})_2O_3$ display a magnetic moments ordering, whereas for $(La_{0.5}Dy_{0.5})_2O_3$ only short range magnetic correlations can be argued, suggesting a possible magnetic moments ordering at lower temperature. $LaErO_3$ is characterized by a magnetic wavevector $\mathbf{k} = (0, 0, 0)$ and forms an antiferromagnetic $G_xC_yA_z$-type structure belonging to the *Pnma* Shubnikov group with a total magnetic moment of 6.78(3) μ_B. The antiferromagnetic structure of $(La_{0.5}Er_{0.5})_2O_3$ is similar to the one typical of Er_2O_3, with a total magnetic moment of 4.28(2) μ_B at both different magnetic sites; it is characterized by $\mathbf{k} = (0, 0, 0)$ and belongs to the magnetic $Ia\bar{3}$ Shubnikov group.

Keywords: neutron diffraction, Rietveld refinement, rare earth oxides, perovskite, soft modes, magnetic structures

(Some figures may appear in colour only in the online journal)

1. Introduction

The magnetic properties of compounds containing Ln^{3+} ions (*Ln*: lanthanide element) are among the most fascinating phenomena in the physical chemistry of solid state materials. In covalent and ionic compounds *Ln* elements generally display the +3 oxidation state, although +2 and +4 oxidation states are also observed in some cases. The varied magnetochemistry of compounds containing Ln^{3+} ions is mainly determined by electrons of the incomplete 4*f* sub-shell, which are shielded by the outermost filled $5s^25p^6$ orbitals. Moreover, the 4*f* electrons are characterized by very contracted radial distribution functions and thus play a marginal role in chemical bonding. Remarkably, in ionic and covalent compounds the electrostatic field of the surrounding ligands removes the degeneracy of the 4*f* orbitals and splits the multiplet energy levels. The suppression of degeneracy of the 4*f* orbitals results in a significant quenching of orbital angular momentum, which is expected to reduce the magnetic moment for $4f^n$ configurations with $n > 7$, as in the case of Dy^{3+} ($4f^9$) and Er^{3+} ($4f^{11}$). Actually, crystal field effects and spin–orbit coupling are competing, even though the magnitude of the spin–orbit coupling largely exceeds the overall crystal field, especially in heavier Ln^{3+} ions. Consequently, the crystal field removes the degeneracy of the ground multiplet determined by the spin–orbit coupling. Moreover, crystal field splitting leads to a Kramers doublet or quartet degenerate ground state in ionic compounds containing Ln^{3+} ions with an odd number of 4*f* electrons (such as Dy^{3+} and Er^{3+}), allowing for magnetic ordering. In conclusion, in each specific case, the resulting magnetic properties

stem from the $4f^n$ configuration, the symmetry of the crystal field (and the relative strength) and the spin-orbit interaction. Usually, in ionic compounds the magnetic exchange interactions among Ln^{3+} ions are of superexchange type. Since magnetic moments are aligned through a combination of intra- and weaker inter-atomic exchange interactions, magnetic transition temperatures are typically of a few Ks.

Lanthanide sesquioxides—Ln_2O_3—display polymorphism and five distinct structures have been identified; in particular, the *A* (space group: $P\bar{3}m1$—164), *B* (space group: $C2/m$—12) and *C* (space group: $Ia\bar{3}$—206) polymorphs are commonly stable below ~2000 °C, whereas the polymorphs *H* and *X* form at higher temperature [1]. These phases are characterized by weak magnetic interactions, as demonstrated by the low values of the Néel temperature (T_N). In particular, magnetic susceptibility measurements reveal that an antiferromagnetic magnetic moments ordering takes place in cubic Dy_2O_3, Yb_2O_3 and Er_2O_3 at $T_N = 1.2$ K, 2.3 K and 3.4 K, respectively [1]. A few neutron diffraction studies were carried out to study magnetism in Ln_2O_3 compounds and only the magnetic structures of the *C*-type Er_2O_3, Tb_2O_3 and Yb_2O_3 oxides were investigated. In *C*-type Er_2O_3 and Yb_2O_3 a noncollinear antiferromagnetic structure occurs, with the moment direction depending on the local symmetry axis [2, 3], whereas in Tb_2O_3 only one of the two Tb^{3+} sub-lattices orders antiferromagnetically at $T_N = 2.4$ K [4]. A theoretical analysis evidenced that magnetic dipole interactions may concur in the stabilization of the magnetic structure, but superexchange interactions mediated by the intervening O atoms could also be active [3].

The ionic radius of the Ln^{3+} cationic species smoothly contracts across the lanthanide series; for this reason, in mixed Ln_2O_3 oxides, where light and heavy lanthanide elements coexist, a favourable ratio among the Ln^{3+} ionic radii can lead to the formation of orthorhombic distorted perovskite-type compounds. Bharathy *et al* [5] and Artini *et al* [6–8] undertook a structural and stability study, correlating the thermodynamic stability of the phase to the Goldschmidt tolerance factor (*t*) for ABO_3 perovskite-type oxides [9]:

$$t = \frac{(R_A + R_O)}{\sqrt{2} \cdot (R_B + R_O)}$$

where R_A, R_B and R_O are the *A*, *B* and oxygen ionic radii, respectively. Recently Qi *et al* [10] observed a linear relationship between the formation enthalpy values of these compounds and *t*, confirming that the structural distortion is the main factor determining their stabilities. Ideal cubic perovskite-type structures are generally stable for *t* close to 1, whereas distortions may develop below this value, decreasing the cell symmetry, as commonly found in interlanthanide perovskites. Since the temperature range marking the stability field of the orthorhombic perovskite results to increase with increasing *t* value, it is possible to drive the formation of the perovskite (or another structural form of the mixed oxide) by acting on the thermal treatment temperature. It is also known that, due to the insufficient size difference between La^{3+} and Dy^{3+}, the perovksite-type $LaDyO_3$ compound does not crystallize, irrespective of the treatment temperature [6]. A magnetic and specific heat investigation carriedr out on numerous

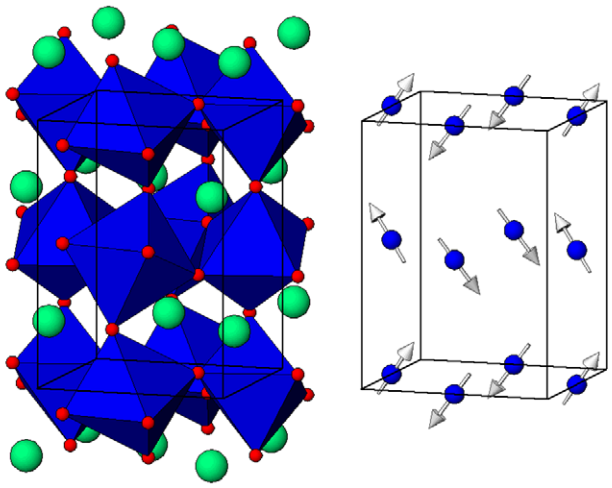

Figure 1. Crystal structure of the orthorhombic $LaErO_3$ phase and the corresponding $G_xC_yA_z$-type magnetic moments ordering at the Er sub-lattice.

Table 1. Structural data obtained for orthorhombic $LaErO_3$ after Rietveld refinement (NPD data collected at 1.5 K).

Space group		*Pnma* (n° 62)		
a (Å)		*b* (Å)		*c* (Å)
6.0434(1)		8.4171(1)		5.8286(1)
Atom	Wyckoff site	*x*	*y*	*z*
La	4*c*	0.0538(1)	¼	0.9758(1)
Er	4*b*	½	0	0
O(1)	4*c*	0.4427(1)	¼	0.1268(1)
O(2)	8*d*	0.3043(1)	0.0674(1)	0.6903(1)
Magnetic space group		*Pnma* (n° 62.441)		
M_x (μ_B)	M_y (μ_B)	M_z (μ_B)		M_{tot} (μ_B)
4.69(3)	4.76(2)	1.16(2)		6.78(3)
R_{Bragg} (%)		R_F (%)	$R_{Magnetic}$ (%)	
3.66		2.22	5.12	

interlanthanide perovskites revealed that $LaYbO_3$, $CeYbO_3$ and $PrYbO_3$ antiferromagnetically order at 2.7 K, whereas $LaErO_3$ at 2.4 K; conversely, $LaHoO_3$, $LaTmO_3$, $CeTmO_3$, $CeLuO_3$, $PrLuO_3$ are paramagnetic down to 1.8 K, whereas $LaLuO_3$ is diamagnetic [11].

Recently our research group carried out an investigation on orthorhombic $LaYbO_3$ and $LaHoO_3$ based on neutron powder diffraction; as a result, it was found out that Yb^{3+} magnetic moments order in $LaYbO_3$ at 2.4 K according to a F_yG_z-type structure, belonging to the $Pn'ma'$ magnetic space group, whereas $LaHoO_3$ is paramagnetic down to 1.5 K [12].

Several studies have been performed in the past about the stability of interlanthanide oxides [13–16] and the magnetic structure of $LaErO_3$ [17], but to the authors' knowledge, the effect of the crystal structure on the magnetic properties of the same interlanthanide mixed oxide has not yet been reported. With the aim to continue the study of the magnetic structures of interlanthanide mixed oxides, in this work we report the results obtained by neutron powder diffraction of cubic

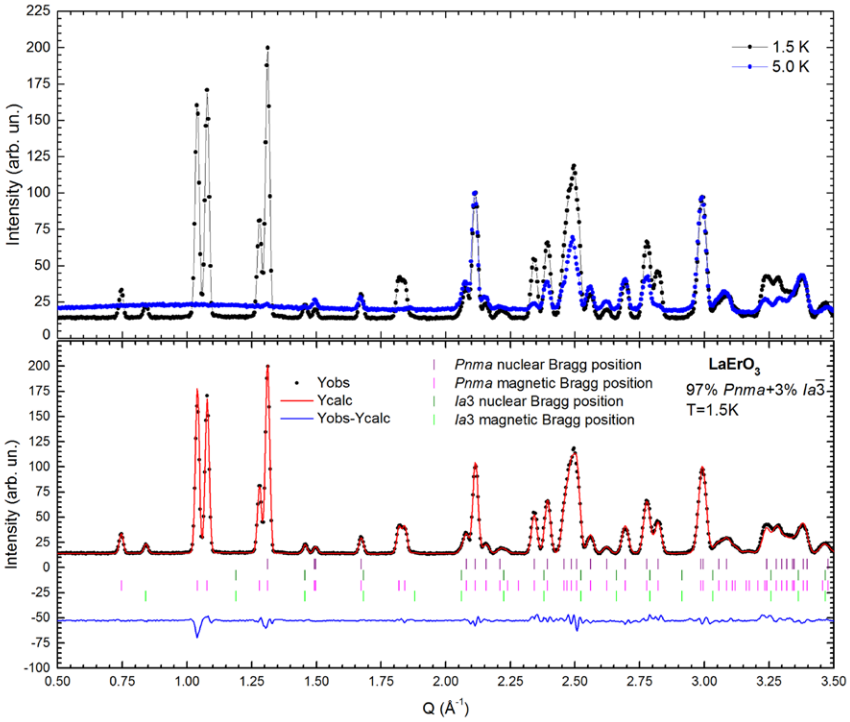

Figure 2. Upper panel: comparison between the NPD patterns collected at 1.5 K and 5 K (normalized data). Lower panel: Rietveld refinement plot obtained for orthorhombic $LaErO_3$ (normalized data collected at 1.5 K).

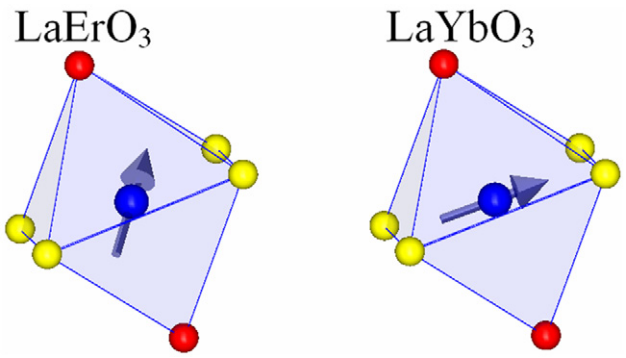

Figure 3. Relationship between the magnetic moment orientation and atomic arrangement in the octahedra pertaining to orthorhombic $LaErO_3$ and $LaYbO_3$; blue, red and yellow spheres represent the magnetic Ln^{3+} ions, axial O(1) and equatorial O(2) oxygens, respectively.

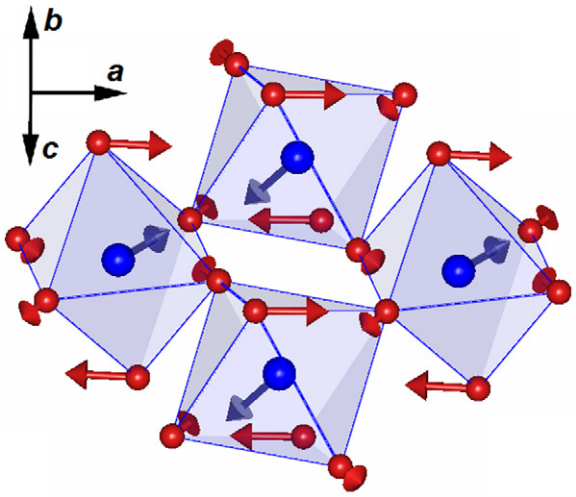

Figure 4. Perspective view showing the relationship between the displacement of O atoms corresponding to the Γ_1^+ mode (represented by red arrows) accompanying magnetic moments ordering and the orientation of the Er^{3+} magnetic moments (blue arrows) in $LaErO_3$; for the sake of clarity La atoms and their displacements are not represented.

$(La_{0.5}Er_{0.5})_2O_3$ and $(La_{0.5}Dy_{0.5})_2O_3$ solid solutions, as well as of orthorhombic $LaErO_3$. In these compounds the Ln^{3+} ions are in a 6-fold coordination, although the coordination polyhedra are different in the cubic and orthorhombic structures. Neutron diffraction provides information about the involved magnetic moments ordering type and the average value of the ordered magnetic moment; these informations are fundamental in order to gain useful insights for the determination of the dominant magnetic interactions activating the cooperative magnetic ordering in these compounds. In particular, our investigation is focused on: 1) the differences occurring when phases with the same chemical composition crystallize with different structures, such as cubic $(La_{0.5}Er_{0.5})_2O_3$ and orthorhombic $LaErO_3$ compounds; 2) the evolution of the magnetic structure when the *Ln* element is changed, as within the isotypic compounds $(La_{0.5}Er_{0.5})_2O_3$ and $(La_{0.5}Dy_{0.5})_2O_3$. In all these compounds Er^{3+} ($4f^{11}$) and Dy^{3+} ($4f^9$) are characterized by an odd number of electrons in the 4*f* external shell, and are therefore Kramer's ions. In this context a first neutron powder diffraction analysis on $LaErO_3$ was carried out in the late '60s, evidencing an antiferromagnetic ordering below 2.4 K, with an $A_xG_yC_z$-type arrangement of the Er^{3+} magnetic moments and a total moment equal to 6.3 μ_B [17].

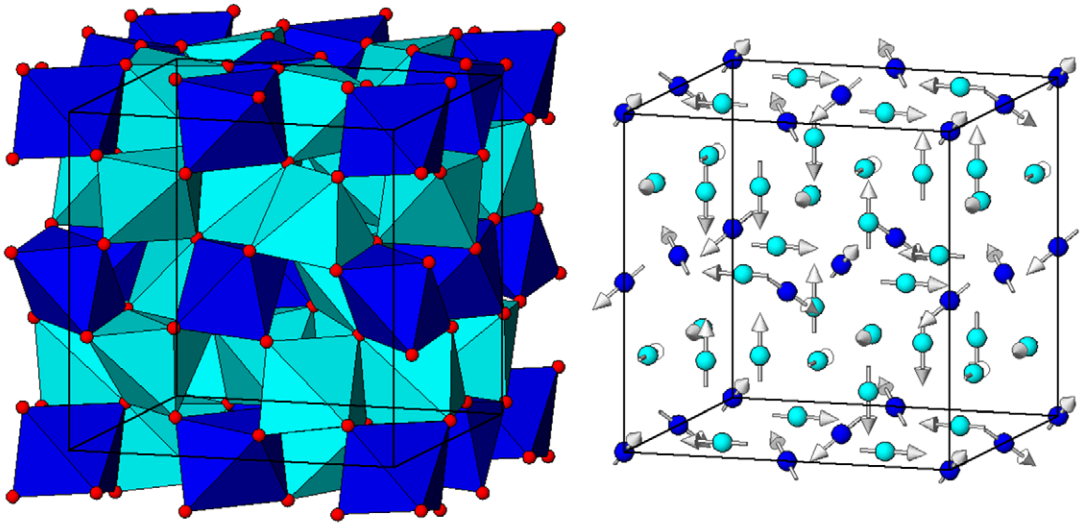

Figure 5. On the left: crystal structure of the cubic $(La_{0.5}Er_{0.5})_2O_3$ and $(La_{0.5}Dy_{0.5})_2O_3$; light and dark blue octahedral are coordinated by Ln^{3+} ions located at 8*a* and 24*d* Wyckoff sites, respectively. On the right: magnetic moments ordering at the Er^{3+} sub-lattices in cubic $(La_{0.5}Er_{0.5})_2O_3$.

More recently, Blanusa *et al* [18]. investigated the magnetic properties of La-Er oxides; they found that in both *A* and *C*-type $(La_{1-x}Er_x)_2O_3$ polymorphs exchange interactions constitute small perturbations and the Er^{3+} ions are less affected by the crystal field, whereas perovskitic $LaErO_3$ is characterized by a more complex behaviour.

2. Methods

Lanthanide mixed oxides were prepared by wet chemistry, with the aim to obtain an optimum homogenization. They were synthesized by coprecipitation of the corresponding mixed oxalates $(La_{0.5}Ln_{0.5})_2[C_2O_4]_3{\cdot}nH_2O$, as described in [19, 20], starting from stoichiometric amounts of La_2O_3 and Ln_2O_3 (Ln = Er, Dy). The latter were dissolved in HCl (13% wt.), the two solutions were mixed, and a large excess of an oxalic acid solution was added, causing an immediate precipitation of the corresponding mixed oxalates. The precipitate was filtered, washed and dried in oven at 363 K overnight. Mixed oxides were then obtained by heating oxalates in air; in particular, perovskitic $LaErO_3$ and both cubic oxides were obtained by treating oxalates at 1473 K for 2 d, and at 873 K for 10 d, respectively. The obtainment of the desired phases was checked by x-ray powder diffraction analysis using a PHILIPS PW1830 diffractometer with Bragg-Brentano geometry.

Neutron powder diffraction analysis (NPD; $\lambda = 2.4500$ Å; step = 0.1 deg) was carried out at the spallation neutron source SINQ of the Paul Scherrer Institute (Villigen, CH) using the high-intensity DMC diffractometer equipped with an Orange He cryostat. NPD patterns were acquired between 1.5 K and 15 K. Rietveld refinement was carried using the program FullProf [21]. The peak shape was modelled with a Thompson-Cox-Hastings pseudo-Voigt function convoluted with axial divergence asymmetry function coupled to an instrumental file; in the final cycle the following parameters were refined: the scale factor; the zero point of detector; the background (5th order polynomial function); the unit cell parameters; the atomic site coordinates not constrained by symmetry; the microstructural parameters; the magnetic moment at the magnetic sites (when magnetic scattering contribution is present).

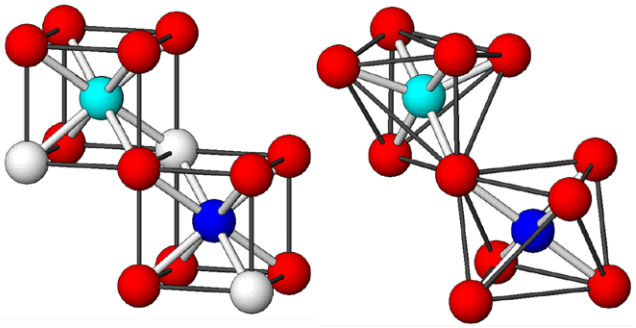

Figure 6. Comparison between a defective fluorite-type structure containing an ordered array of 25% of vacancies at the O site (on the left) and the bixbyite-type structure (on the right); red, white, blue and pale blue spheres represents oxygen, vacancies and Ln^{3+} ions (blue and pale blue spheres are Ln^{3+} ions at the 8*a* and 24*d* sites of the bixbyite-type structure, respectively).

Magnetic moment orderings were deduced by using the irreducible representations (*irrep*) analysis [22]: the allowed magnetic structures were calculated using the BasIReps program included in the FullProf suite and the SARAh program [23]. Finally the agreement between the observed and calculated diffraction patterns was checked.

3. Results and discussion

3.1. Orthorhombic $LaErO_3$

At room temperature orthorhombic $LaErO_3$ crystallizes in the *Pnma* space group (space group number 62) and isotypic with $GdFeO_3$ (figure 1). As proved by Rietveld refinement, this structural model nicely fits data collected down to 1.5 K

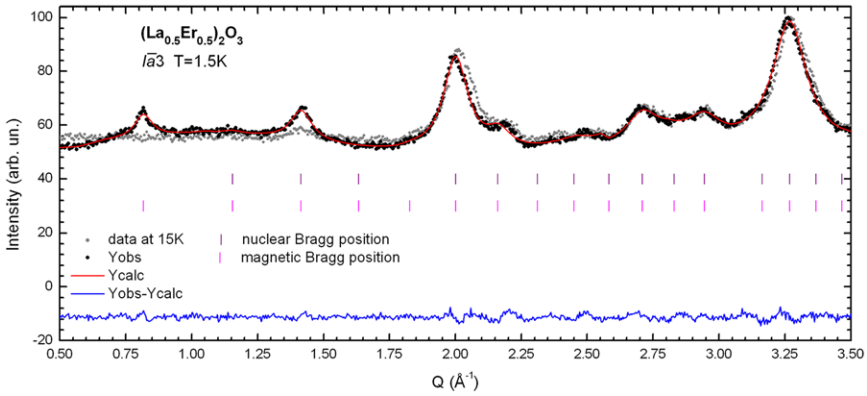

Figure 7. Rietveld refinement plot obtained for cubic $(La_{0.5}Er_{0.5})_2O_3$ (normalized data collected at 1.5 K); normalized data collected at 15 K in the paramagnetic field are superposed for comparison.

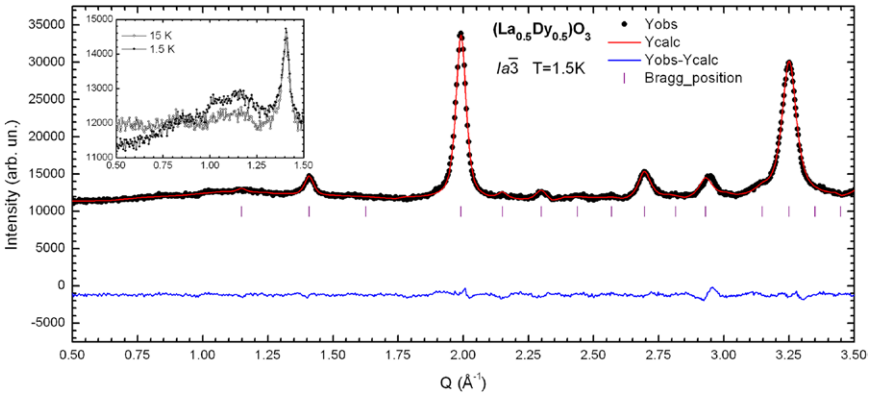

Figure 8. Rietveld refinement plot for cubic $(La_{0.5}Dy_{0.5})_2O_3$ (data collected at 1.5 K); the inset shows the superposition of the NPD patterns collected at 15 K and 1.5 K in the low **Q** region, where a bump is present, originated by magnetic scattering due to magnetic short range correlations at the lower temperature.

Table 2. Structural data obtained for the cubic solid solutions $(La_{0.5}Er_{0.5})_2O_3$ and $(La_{0.5}Dy_{0.5})_2O_3$ after Rietveld refinement (NPD data collected at 1.5 K).

Space group		$Ia\bar{3}$ (n° 206)					
Composition a (Å)		$(La_{0.5}Er_{0.5})_2O_3$ 10.8687(4)			$(La_{0.5}Dy_{0.5})_2O_3$ 10.9343(1)		
Atom	Wyckoff site	x	y	z	x	y	z
$Ln(1)$	8a	0	0	0	0	0	0
$Ln(2)$	24d	0.2821(1)	0	¼	0.2752(1)	0	¼
O	48e	0.0828(1)	0.3788(1)	0.1232(2)	0.0892(1)	0.3690(1)	0.1292(2)
Magnetic space group		$Ia\bar{3}$ (n° 206.37)			/		
M_{tot} @ 8a (μ_B)		4.28(2)			/		
M_{tot} @ 24d (μ_B)		4.28(2)			/		
R_{Bragg} (%)		4.14			1.48		
R_F (%)		2.37			1.37		
$R_{Magnetic}$ (%)		6.67			/		

as well, indicating no structural transformation on cooling. In this structure the smaller Er^{3+} ion is in 6-fold coordination and located at the centre of an octahedron, whereas the larger La^{3+} ion displays a 12-fold coordination. The octahedral tilting in $LaErO_3$ corresponds to the $a^+b^-b^-$ system (N. 10) proposed by Glazer for perovskite structures [24], as in $LaYbO_3$ and $LaHoO_3$ [12].

A closer inspection of the fitted patterns reveals the presence of a very few amounts of a secondary cubic $(La, Er)_2O_3$ solid solution, ~2–3 vol% as estimated by Rietveld refinement. The presence of this phase is particularly evident in the data collected at 1.5 K, as it originates weak but noticeable magnetic peaks that cannot be related to the magnetic moments ordering occurring within the orthorhombic phase.

Table 3. Irreducible representations of $Ia\bar{3}$ space group for propagation vector $\mathbf{k} = (0, 0, 0)$; α and β represent the phase factors for atoms of the same orbit for complex *irreps*, whereas *a*–*n* are 3×3 matrices defining the 3D characters; h_n represents the point operation in Kovalev notation given by $\boldsymbol{R}$ in the symmetry operation $\{\boldsymbol{R}|\boldsymbol{v}\}$ [25].

T_h	Point group rotational elements in Kovalev notation																							
Irrep	h_1	h_2	h_3	h_4	h_5	h_6	h_7	h_8	h_9	h_{10}	h_{11}	h_{12}	h_{25}	h_{26}	h_{27}	h_{28}	h_{29}	h_{30}	h_{31}	h_{32}	h_{33}	h_{34}	h_{35}	h_{36}
Γ_1	1	1	1	1	1	1	1	1	1	1	1	1	1	1	1	1	1	1	1	1	1	1	1	1
Γ_2	1	1	1	1	1	1	1	1	1	1	1	1	-1	-1	-1	-1	-1	-1	-1	-1	-1	-1	-1	-1
Γ_3	1	1	1	1	α	α	α	α	β	β	β	β	1	1	1	1	α	α	α	α	β	β	β	β
Γ_4	1	1	1	1	α	α	α	α	β	β	β	β	-1	-1	-1	-1	$-\alpha$	$-\alpha$	$-\alpha$	$-\alpha$	$-\beta$	$-\beta$	$-\beta$	$-\beta$
Γ_5	1	1	1	1	β	β	β	β	α	α	α	α	1	1	1	1	β	β	β	β	α	α	α	α
Γ_6	1	1	1	1	β	β	β	β	α	α	α	α	-1	-1	-1	-1	$-\beta$	$-\beta$	$-\beta$	$-\beta$	$-\alpha$	$-\alpha$	$-\alpha$	$-\alpha$
Γ_7	*a*	*b*	*c*	*d*	*e*	*f*	*g*	*h*	*i*	*l*	*m*	*n*	$-a$	$-b$	$-c$	$-d$	$-e$	$-f$	$-g$	$-h$	$-i$	$-l$	$-m$	$-n$
Γ_8	*a*	*b*	*c*	*d*	*e*	*f*	*g*	*h*	*i*	*l*	*m*	*n*	*a*	*b*	*c*	*d*	*e*	*f*	*g*	*h*	*i*	*l*	*m*	*n*

Table 4. Shubnikov groups and magnetic space groups number corresponding to the *irreps* of $Ia\bar{3}$ for $\mathbf{k} = (0, 0, 0)$.

Irrep	Shubnikov group	Magnetic space group number
Γ_1	$Ia\bar{3}$	206.37
Γ_2	$Ia'\bar{3}'$	206.39
Γ_3	*Ibca*	73.548
Γ_4	$Ib'c'a'$	73.552
Γ_5	*Ibca*	73.548
Γ_6	$Ib'c'a'$	73.552

No magnetic peaks can be detected in the diffraction pattern collected at 5 K, indicating a paramagnetic state at this temperature. In agreement with previous findings reporting $T_N = 2.4$ K [11, 17], NPD data collected at 1.5 K are characterized by the presence of magnetic peaks due to magnetic moments ordering in $LaErO_3$; no evidence for structural change can be detected (figure 2; upper panel). Moreover, paramagnetic diffuse scattering clearly stands out by comparing the NPD patterns collected at 5 K and 1.5 K, falling off with the increase of the scattering vector **Q**. Weak magnetic peaks due to magnetic ordering in the cubic $(La,Er)_2O_3$ solid solution are also present. In the unit cell of orthorhombic $LaErO_3$ (figure 1, on the left), the Er^{3+} ions are located at the 4*b* Wyckoff site and their magnetic moments order according the Γ_1 *irrep* with $\mathbf{k} = (0, 0, 0)$ to form an antiferromagnetic $G_xC_yA_z$-type structure that belongs to the *Pnma* Shubnikov group (group number 62.441). Figure 1, on the right, depicts the magnetic moments ordering characterizing the Er sublattice of orthorhombic $LaErO_3$, whereas the lower panel of figure 2 shows the Rietveld refinement plot obtained using data collected at 1.5 K. The magnetic structure and the refined magnetic moments (table 1) are in agreement with previous investigations [17].

In $LaErO_3$ magnetic moments approximately lie in a plane formed by the two axial O(1) atoms and two equatorial O(2) ones, pointing towards the centre of one of the octahedron edges. This arrangement is somehow similar to that detected in $LaYbO_3$, despite its different magnetic structure (F_yG_z-type ordering) [12]: here the ordered magnetic moments lie in the plane formed by the four O(2) atoms, but also in this case the moments point towards the centre of one of the octahedron edges (figure 3).

By comparing the crystal structures at 5 K and 1.5 K, the symmetry mode analysis evidences a notable change of the global amplitude of the non-symmetry breaking Γ_1^+ (A_g) mode (0.121(1) Å).

Figure 4 shows the nice relationship between the displacement of O atoms and the orientation of the Er^{3+} magnetic moments; Er^{3+} ions experience no displacement on cooling, since they are fixed by symmetry. As the intervening O atoms play a fundamental role when superexchange interactions are active, their displacements connected with the Er^{3+} magnetic moments orientation may support a scenario foreseeing the involvement of superexchange interactions for the obtainment of the magnetic ground state in this compound. This hypothesis is corroborated by the fact that the coordination number of Er^{3+} ions is not so high for reducing the strength of the superexchange interactions. In any case further analyses are needed in order to gain more certain conclusions. For comparison, a similar symmetry mode analysis was carried out for the isotypic $LaYbO_3$ and $LaHoO_3$ compounds, using data collected at 4 K and 1.5 K in a previous experiment [12]; noteworthy, $LaYbO_3$ displays an antiferromagnetic F_yG_z-type ordering at 2.4 K, with a total magnetic moment of 0.87 μ_B, whereas $LaHoO_3$ is paramagnetic down to 1.5 K [12]. In both $LaYbO_3$ and $LaHoO_3$ the displacement of O atoms is almost negligible and the global amplitudes of the Γ_1^+ mode are only 0.018(1) Å and 0.024(2) Å, respectively, indicating that no relevant structural change couples with magnetic moments ordering in $LaYbO_3$. These different behaviours may be likely ascribed to the different mechanisms activating cooperative magnetism in these compounds.

3.2. Cubic $(La_{0.5}Er_{0.5})_2O_3$ and $(La_{0.5}Dy_{0.5})_2O_3$ solid solutions

Cubic $(La_{0.5}Er_{0.5})_2O_3$ and $(La_{0.5}Dy_{0.5})_2O_3$ are actually solid solutions pertaining to the pseudo-binary La_2O_3—Er_2O_3 and La_2O_3—Dy_2O_3 systems, respectively; they crystallize in the $Ia\bar{3}$ space group (space group number 206) and are isotypic with bixbyite—$(Mn_{0.5}Fe_{0.5})_2O_3$. The bixbyite-type structure is closely related to the fluorite-type structure, where ¼ of the anion sites are systematically substituted by an ordered array of vacancies and the remaining atoms are slightly rearranged. The *Ln* ions are distributed at the 8*a* and 24*d* Wyckoff sites (C_{3i} and C_2 point group symmetry in Schoenflies notation, respectively): they are both 6-fold coordinated and form a complex network of edge and corner sharing irregular octahedral polyhedra (figure 5, on the left); O atoms display a 4-fold coordination, giving rise to an edge sharing network of slightly distorted tetrahedra. Figure 6 shows the close relationship between the bixbyite- and fluorite-type structure. In the bixbyite-type structure the Ln^{3+} ion is 6-fold coordinated, instead of the 8-fold coordination taking place in the fluorite-type structure. The cubic coordination polyhedron around the Ln^{3+} ion at the 8*a* Wyckoff site has two vacancies along a face diagonal, whereas that around the Ln^{3+} ion at the 24*d* site has two vacancies along a body diagonal (figure 6).

The crystallization degree of the analyzed samples is quite low, as evidenced by a marked broadening of the diffraction lines (figures 7 and 8); the microstructural analysis carried out by Rietveld refinement reveals that the average size of the diffracting domains is ~7 nm and ~13 nm in $(La_{0.5}Er_{0.5})_2O_3$ and $(La_{0.5}Dy_{0.5})_2O_3$, respectively. The lattice parameters decrease with the increase of the *Ln* atomic number on account of the lanthanide contraction, i.e. moving from $(La_{0.5}Dy_{0.5})_2O_3$ to $(La_{0.5}Er_{0.5})_2O_3$ (table 2).

The NPD pattern of $(La_{0.5}Er_{0.5})_2O_3$ collected at 1.5 K displays evident magnetic Bragg peaks (figure 7). A significant paramagnetic scattering contribution to the background results by comparing the NPD patterns collected at 15 K and 1.5 K, particularly at the lowest **Q**; remarkably this contribution is still present to some extent even at 1.5 K, indicating the persistence of a notable amount of magnetic moments randomly oriented.

The magnetic structure of $(La_{0.5}Er_{0.5})_2O_3$ is characterized by a magnetic propagation wave-vector $\mathbf{k} = (0, 0, 0)$, so that the magnetic unit cell is the same as the nuclear one. The corresponding *irreps* for the $Ia\bar{3}$ space group were calculated using the programs BasIReps and SARAh [21, 23]. Table 3 shows that there are two 1D *irreps*, four complex *irreps* and two 3D *irreps*. The decomposition of the global magnetic representation for the two 8*a* and 24*d* Wyckoff sites occupied by Er^{3+} ions is:

$$\Gamma_m(8a) = 1\Gamma_1 \oplus 1\Gamma_3 \oplus 1\Gamma_5 \oplus 3\Gamma_8$$

$$\Gamma_m(24d) = 1\Gamma_1 \oplus 1\Gamma_2 \oplus 1\Gamma_3 \oplus 1\Gamma_4 \oplus 1\Gamma_5 \oplus 1\Gamma_6 \oplus 5\Gamma_7 \oplus 5\Gamma_8$$

Only the representations Γ_1 and Γ_2 describe real magnetic structures for this system; on the other hand when more than one magnetic site is present, the magnetic ordering is in principle driven by a single *irrep*. In the present case only Γ_1 appears in the decomposition of the global magnetic representation for both sites and describes a real magnetic structure; in addition, only one free parameter is present if this single *irrep* defines the magnetic structure. Rietveld refinement of the data collected at 1.5 K (table 2) confirms that the magnetic transition in cubic $(La_{0.5}Er_{0.5})_2O_3$ is connected to a single active Γ_1 *irrep*, in agreement with the Landau theory for the 2nd order phase transition. The resultant noncollinear antiferromagnetic structure (represented in figure 5, on the right) belongs to the $Ia\bar{3}$ Shubnikov group (group number 206.37; table 4) and is thus similar to that developing in pure Er_2O_3 [2, 3]; the magnetic anisotropy is strictly related to the distribution of the O vacancies as well as to the local symmetry of the Er^{3+} sites. Unfortunately, the sample quality prevents an independent refinement of the magnetic moments at the two sites; on the other hand, in pure Er_2O_3 the magnitudes of the magnetic moment at the two sub-lattices are very similar [2, 3]; for these reasons the magnetic moments at the two Er^{3+} sites were constrained to a same value during refinement. In agreement with the remarkable amount of paramagnetic scattering still present at 1.5 K, the refined values for ordered magnetic moments ($4.28\mu_B$, table 2) are significantly smaller than those measured in pure Er_2O_3 ($5.4–6.0\mu_B$ [2, 3]), likely on account of the dilution with non-magnetic La^{3+}.

Low temperature heat-capacity measurements on Er_2O_3 suggested that antiferromagnetic ordering is decoupled at the two Er^{3+} sites, with ions at the 8*a* site ordering at 3.3 K and those at the 24*d* site below 2 K [26]. In this scenario it could be supposed that the Bragg magnetic peaks observed at 1.5 K in the present experiment arise due to ordering at the 8*a* sub-lattice only. An attempt to refine the magnetic structure with this structural model results in a large increase of the magnetic *R* factor ($R_{\text{Magnetic}} = 11.1\%$), clearly indicating its inconsistency.

No magnetic Bragg peaks are present in the NPD pattern of the cubic $(La_{0.5}Dy_{0.5})_2O_3$ solid solution collected at 1.5 K. Nonetheless, a clear bump at low **Q** values emerges, even though this feature (with a reduced intensity) can be already appreciated in the data collected at 15 K (figure 8). An antiferromagnetic ordering is reported at 1.2 K for the pure cubic end-member Dy_2O_3 [1]; the formation of this bump suggests the occurrence of short range magnetic correlations that are progressively enhanced on cooling. This conclusion is supported by the observation that the increase of the bump intensity is coupled with a decrease in the paramagnetic scattering contribution at low **Q**, indicating a significant decrease of the random orientation of the magnetic moments. In this context it is worth to note that the magnetic structure of the sc oxide Dy_2O_3 has not yet been investigated by NPD analysis, to our knowledge.

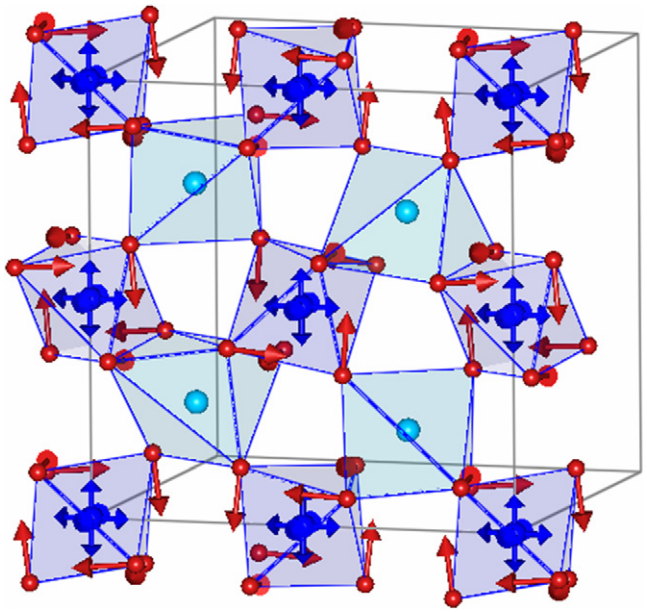

Figure 9. Description of the Γ_1^+ distortion component for $(La_{0.5}Er_{0.5})_2O_3$; the directions of the arrows correspond to atomic displacements.

As afore mentioned, a theoretical analysis suggested that superexchange interactions among Er^{3+} ions could be active in Er_2O_3 [3]. As in $LaErO_3$, in principle the coordination numbers of the Ln^{3+} ions in these compounds are not so high to reduce the effectiveness of the superexchange interactions. By comparing the structural data at 15 K and 1.5, the symmetry mode analysis reveals that both $(La_{0.5}Er_{0.5})_2O_3$ and $(La_{0.5}Dy_{0.5})_2O_3$ exhibit significant changes of the global amplitude of the non-symmetry breaking Γ_1^+ (A_g) mode, being 1.141(5) Å and 0.283(5) Å, respectively. The much larger amplitude detected for $(La_{0.5}Er_{0.5})_2O_3$ may be ascribed to the onset of the superexchange interactions, that can play an effective role in distorting the crystal structure; on the other hand, also $(La_{0.5}Dy_{0.5})_2O_3$ exhibits a significant distortion, that can be related to some extent to the onset of the short-range magnetic interactions. Nonetheless, further in-depth investigations are required in order to ascertain the actual occurrence and effective role of superexchange interactions in these compounds. In figure 9 a slab of the $(La_{0.5}Er_{0.5})_2O_3$ structure is represented, showing the displacement of the atoms (O and *Ln* atoms at 24*d* site) according to the Γ_1^+ mode (vibrations of *Ln* atoms at 24*d* site are along cubic axes and thus triply degenerate). Displacement of *Ln* atoms at the 8*a* site are obviously prevented by symmetry.

4. Conclusions

The structural and magnetic properties of $LaErO_3$, $(La_{0.5}Er_{0.5})_2O_3$ and $(La_{0.5}\ Dy_{0.5})_2O_3$ oxides were examined by neutron powder diffraction between 1.5 K and 15 K. In the orthorhombic $LaErO_3$ phase an antiferromagnetic $G_xC_yA_z$ magnetic moments ordering takes place at the Er sub-lattice, characterized by a total magnetic moment of 6.78(3) μ_B; this magnetic structure belongs to the *Pnma* Shubnikov group. Despite the large dilution at the Er^{3+} site with non magnetic Ln^{3+}, an antiferromagnetic ordering occurs in $(La_{0.5}Er_{0.5})_2O_3$, exhibiting the same magnetic moments arrangement characterizing Er_2O_3; this magnetic structure belongs to the magnetic $Ia\bar{3}$ Shubnikov group. In $(La_{0.5}\ Dy_{0.5})_2O_3$ long-range magnetic ordering is not detected down to 1.5 K; on the other hand evidences for short-range magnetic correlations are observed.

As cooperative magnetism sets in, a remarkable atomic re-arrangement occurs both in $LaErO_3$ and $(La_{0.5}Er_{0.5})_2O_3$; in particular, atomic displacements mainly affect the intervening O atoms.

Acknowledgments

Dr Marcella Pani (University of Genova) is kindly acknowledged for her help in preparing samples. This work is based on experiments performed at the Swiss spallation neutron source SINQ, Paul Scherrer Institute, Villigen, Switzerland.

References

[1] Eyring L R 1979 The binary rare earth oxides *Handbook on the Physics and Chemistry of Rare Earths* vol 3 (New York: North-Holland) p 337
[2] Bertaut E-F and Chevalier R 1966 *C. R. Acad. Sci., Paris* **B262** 1707
[3] Moon R M, Koehler W C, Child H R and Raubenheimer L J 1968 *Phys. Rev.* **176** 722
[4] Quezel S, Bertaut E F and Quezel G 1969 *Colloques sur les Eléments de Terre Rare* (Grenoble: C.N.R.S.)
[5] Bharathy M, Fox A H, Mugavero S J and zur Loye H C 2009 *Solid State Sci.* **11** 651
[6] Artini C, Costa G A, Carnasciali M M and Masini R 2010 *J. Alloys Compd.* **494** 336
[7] Artini C, Costa G A and Masini R 2011 *J. Therm. Anal. Calorim.* **103** 17
[8] Artini C, Pani M, Lausi A and Costa G A 2016 *J. Phys. Chem. Solids* **91** 93–100
[9] Goldschmidt V M 1926 *Naturwissenschaften* **14** 477
[10] Qi J, Guo X, Navrotsky A 2015 *J. Solid State Chem.* **227** 150
[11] Ito K, Tezuka K, Hinatsu Y 2001 *J. Solid State Chem.* **157** 173
[12] Martinelli A, Masini R, Artini C, Costa G A and Keller L 2013 *J. Phys.: Condens. Matter* **25** 426005
[13] Bevan D J M and Summerville E 1979 Mixed rare earth oxides *Handbook on the Physics and Chemistry of Rare Earths* vol 3 (New York: North-Holland) p 401
[14] Berndt U, Maier D and Keller C 1975 *J. Solid State Chem.* **13** 131
[15] Coutures J, Rouanet A, Verges R and Foex M 1976 *J. Solid State Chem.* **17** 171
[16] Coutures J and Coutures J P 1976 *J. Solid State Chem.* **19** 29
[17] Moreau J M, Mareschal J and Bertaut E F 1968 *Solid State Commun.* **6** 751
[18] Blanusa J, Mitric M, Felner I, Jovic N and Bradaric I 2003 *J. Magn. Magn. Mater.* **263** 295
[19] Costa G A, Artini C, Ubaldini A, Carnasciali M M, Mele P and Masini R 2008 *J. Therm. Anal. Calorim.* **92** 101
[20] Ubaldini A, Artini C, Costa G A, Carnasciali M M and Masini R 2008 *J. Therm. Anal. Calorim.* **91** 797
[21] Rodríguez-Carvajal J 1993 *Physica* B **192** 55
[22] Bertaut E F 1968 *Acta Cryst.* A **24** 217
[23] Wills A S 2000 *Physica* B **276** 680
[24] Glazer M 1975 *Acta Cryst.* A **31** 756
[25] Kovalev O V 1993 *Representations of the Crystallographic Space Groups* ed H T Stokes and D M Hatch (Gordon and Breach Science Publishers)
[26] Tang Y J, Cao X W, Ho J C and Ku H C 1992 *Phys. Rev.* B **46** 1213